ISSN 1063-7788, Physics of Atomic Nuclei, 2007, Vol. 70, No. 6, pp. 1058–1073. © Pleiades Publishing, Ltd., 2007.
Original Russian Text © K.E. Shestermanov, A.N. Vasiliev, J. Butler, A.A. Derevschikov, P. Kasper, V.V. Kiselev, V.I. Kravtsov, Y. Kubota, R. Kutschke, Yu.A. Matulenko, N.G. Minaev, V.V. Mochalov, D.A. Morozov, L.V. Nogach, M. Rovere, A.V. Ryazantsev, P.A. Semenov, S. Stone, A.V. Uzunian, J. Yarba, 2007, published in Yadernaya Fizika, 2007, Vol. 70, No. 6, pp. 1093–1108.

ELEMENTARY PARTICLES AND FIELDS
Experiment

Expected Accuracy in a Measurement of the CKM Angle α Using a Dalitz Plot Analysis of $B^0 \to \rho\pi$ Decays in the BTeV Project

K. E. Shestermanov[†1)], A. N. Vasiliev[1)*], J. Butler[2)], A. A. Derevschikov[1)], P. Kasper[2)], V. V. Kiselev[1)], V. I. Kravtsov[1)], Y. Kubota[3)], R. Kutschke[2)], Yu. A. Matulenko[1)], N. G. Minaev[1)], V. V. Mochalov[1)], D. A. Morozov[1)], L. V. Nogach[1)], M. Rovere[4)], A. V. Ryazantsev[1)], P. A. Semenov[1)], S. Stone[5)], A. V. Uzunian[1)], and J. Yarba[2)]

Received March 28, 2006; in final form, August 30, 2006

Abstract—A precise measurement of the angle α in the CKM triangle is very important for a complete test of Standard Model. A theoretically clean method to extract α is provided by $B^0 \to \rho\pi$ decays. Monte Carlo simulations to obtain the BTeV reconstruction efficiency and to estimate the signal-to-background ratio for these decays were performed. Finally the time-dependent Dalitz-plot analysis, using the isospin amplitude formalism for tree and penguin contributions, was carried out. It was shown that in one year of data taking BTeV could achieve an accuracy on α better than 5°.

PACS numbers: 11.30.Hv, 12.15.Hh, 13.25.Hw
DOI: 10.1134/S1063778807060087

Dedicated to the memory of Konstantin Shestermanov, who has made the main contribution to this paper

1. INTRODUCTION

The Standard Model (SM) [1] which incorporates the quark mixing Cabibbo–Kabayashi–Maskawa (CKM) mechanism [2] has been increasingly successful, supported with many precise experimental results. This strongly indicates that, at low energies, the SM is the effective description of Nature. However, there are reasons to believe that there exists physics beyond the SM. For example, from the astrophysical point of view, it is a serious problem that the matter–antimatter asymmetry in the Universe cannot be explained solely from the CP violation in the SM, which originates from quark flavor mixing. This observation, together with others, leads one to believe that there is a new physics, most likely, at the TeV energy scale. One of the critical measurements to test the SM or to obtain strong indications of new physics are precisie measurements of the angles in the Unitary Triangles (UT), which are of non-zero area if CP violation exists.

A unique program that would have allowed one to challenge the SM explanation of CP violation, mixing and rare decays in the b- and c-quark system was proposed by the BTeV project [3] at the Tevatron at Fermilab. The design of BTeV exceled in several crucial areas including: triggering on decays with purely hadronic final states, charged-particle identification, excellent electromagnetic calorimetry and excellent proper time resolution. Exploiting the large number of b's and c's produced at the Tevatron collider, the experiment would have provided precise measurements of SM parameters and an exhaustive search for physics beyond the SM. The complete physics objectives of BTeV included measuring the CP-violating angles α, β, and γ of the UT. In particular, the measurement of α is difficult due to small overall rates and because the gluonic penguin rates are of the same order as the tree rates, causing well-known difficulties in extracting the weak phase angle. Quinn and Snyder [4] have suggested a theoretically clean method to extract α from decays of the type $B^0 \to \rho\pi$. The final state of these decays is not a CP eigenstate, which results in the need of a Dalitz-plot analysis. We focus on the measurement of α, via collecting a large sample of $B^0 \to (\rho\pi)^0$ decays. Direct measurements from the B factories demonstrate that

[†]Deceased.
[1)]Institute for High Energy Physics, Protvino, Russia.
[2)]Fermilab, Batavia, USA.
[3)]University of Minnesota, Minneapolis, USA.
[4)]Istituto Nazionale di Fisica Nucleare, Sez. di Milano, Italy.
[5)]Syracuse University, USA.
[*]E-mail: Alexander.Vasiliev@ihep.ru

the average hh decays (where $h = (\rho, \pi)$) are known to a precision of $O(10^\circ)$ [5], with the use of isospin. In this paper we demonstrate that BTeV could have done the measurement with a much better precision.

The paper is organized as follows. Section 2 provides brief introduction of the CKM matrix. In Section 3 we give a general overview of the BTeV project. In Sections 4 and 5, respectively, we report on the expected reconstruction efficiencies and the signal/background ratio of the $B^0 \to (\rho\pi)^0$ decays in BTeV. Section 6 covers the phenomenological formalism of $B^0 \to (\rho\pi)^0$ decays. In Section 7 we describe results of the time-dependent Dalitz-plot analysis of the simulated $B^0 \to (\rho\pi)^0$ decays in BTeV.

2. THE CKM MATRIX AND THE ANGLE α

In the SM there are three generations of leptons and quarks. The physical point-like particles that have both strong and electroweak interactions, the quarks, are mixtures of weak eigenstates, described by a 3×3 unitary matrix, called the CKM matrix [2],

$$\begin{pmatrix} d' \\ s' \\ b' \end{pmatrix} = \begin{pmatrix} V_{ud} & V_{us} & V_{ub} \\ V_{cd} & V_{cs} & V_{cb} \\ V_{td} & V_{ts} & V_{tb} \end{pmatrix} \begin{pmatrix} d \\ s \\ b \end{pmatrix}. \quad (1)$$

The unprimed states are the mass eigenstates, while the primed states denote the weak eigenstates. The V_{ij}'s are complex numbers that can be expressed in terms of four independent real quantities. These numbers are fundamental constants of Nature that need to be determined from experiment. In the Wolfenstein approximation the matrix is written as [6]

$$V_{\rm CKM} = \begin{pmatrix} 1 - \lambda^2/2 & \lambda & A\lambda^3(\rho - i\eta(1 - \lambda^2/2)) \\ -\lambda & 1 - \lambda^2/2 - i\eta A^2\lambda^4 & A\lambda^2(1 + i\eta\lambda^2) \\ A\lambda^3(1 - \rho - i\eta) & -A\lambda^2 & 1 \end{pmatrix}, \quad (2)$$

where (λ, A, ρ, η) are four mixing parameters with $\lambda = |V_{us}| \approx 0.22$, $A \approx 0.8$ (measured using semileptonic s and b decays [7]), and η represents the CP-violating phase. This expression is accurate to order λ^3 in the real part and λ^5 in the imaginary part. It is necessary to express the matrix to this order to have a complete formulation of the physics we wish to pursue.

The unitarity of the CKM matrix leads to various relations among the matrix elements:

$$V_{ud}V_{us}^* + V_{cd}V_{cs}^* + V_{td}V_{ts}^* = 0, \quad (3)$$

$$V_{us}V_{ub}^* + V_{cs}V_{cb}^* + V_{ts}V_{tb}^* = 0, \quad (4)$$

$$V_{ub}V_{ud}^* + V_{cb}V_{cd}^* + V_{tb}V_{td}^* = 0, \quad (5)$$

that can be geometrically represented in the complex plane as triangles. These are UT, though the term "unitary triangle" is usually reserved only for the bd triangle in (5), where the angles are all thought to be relatively large. This CKM triangle is depicted in Fig. 1. It shows the angles α, β, and γ. These angles are defined as

$$\alpha = \arg\left[-\frac{V_{td}V_{tb}^*}{V_{ud}V_{ub}^*}\right], \quad (6)$$

$$\beta = \arg\left[-\frac{V_{cd}V_{cb}^*}{V_{td}V_{tb}^*}\right], \quad \gamma = \arg\left[-\frac{V_{ud}V_{ub}^*}{V_{cd}V_{cb}^*}\right]$$

and can be determined by measuring CP violation in B decays.

They can roughly be divided in two classes :

decays that are expected to have relatively small direct CP violation and hence are particularly interesting for extracting CKM parameters from interference of decays with and without mixing;

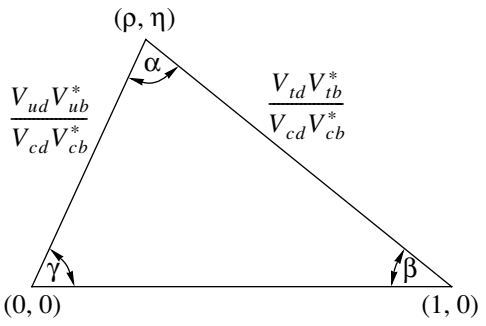

Fig. 1. Unitary Triangle.

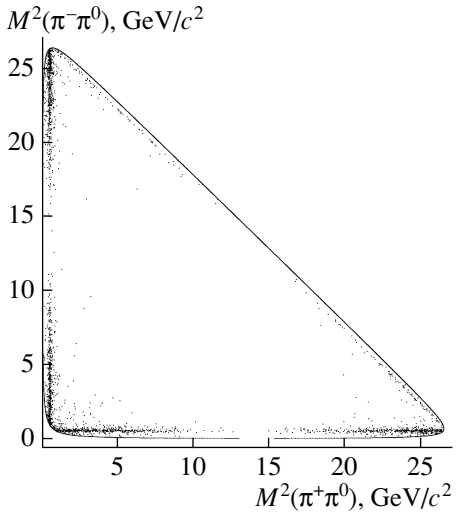

Fig. 2. The Dalitz plot for $B^0 \to \rho\pi \to \pi^+\pi^-\pi^0$.

decays in which direct CP violation could be significant and therefore that cannot be cleanly interpreted in terms of CKM phases.

B decays used to extract β belong to the first group, whereas decays that have been considered to measure α belong to the second one.

The primary source for measurements of $\sin(2\beta)$ are the decays of the type $b \to c\bar{c}s$. The most statistically significant measurements of CP violation in the B system were made by BABAR [8] and BELLE [9], resulting in the average value of $\sin(2\beta) = 0.725 \pm 0.037$ [10].

Measuring α is more difficult than measuring β in several respects. First of all, the decay amplitudes are modulated by V_{ub} rather than V_{cb} making the overall rates small, of the order of 10^{-5} to 10^{-6}. Secondly, the gluonic penguin rates are of the same order as the trees causing large theoretical uncertainties in cleanly extracting α from asymmetry measurements alone.

The decay $B^0 \to \pi^+\pi^-$ has been proposed as a way to measure $\sin(2\alpha)$. However, the penguin pollution is quite large and cannot be ignored. Gronau and London [11] have shown that an isospin analysis using the additional decays $B^- \to \pi^-\pi^0$ and $B^0 \to \pi^0\pi^0$ can be used to extract α [12], but the $\pi^0\pi^0$ final state is extremely difficult to detect in any existing or proposed experiment. $B \to \pi\pi$ has been seen but there is no B-decay vertex information, therefore there is no way to perform a time-dependent CP-violation measurement. In fact, the data that does exist has been used to limit the penguin contribution to these decays, but the limit is not very restrictive. Lipkin, Nir, Quinn, and Snyder [13] have extended the analysis in [11] to include other decays, among them $B \to \rho\pi$. Snyder and Quinn [4] subsequently extended that work and proposed not only an isospin analysis, but a full, time dependent, Dalitz-plot study of $B \to \rho\pi$ decay to measure α.

A sample Dalitz plot is shown in Fig. 2. A striking feature of this Dalitz plot is that the events are concentrated close to the kinematic boundary, especially in the corners. This kind of distribution is good for maximizing the interference, which helps minimize the errors. Furthermore, little information is lost by excluding the Dalitz-plot interior, a good way to reduce backgrounds.

Snyder and Quinn [4] have performed an idealized Dalitz plot analysis that uses 1000 or 2000 flavor-tagged background-free events. Trials using 1000 events usually yield good results for α, but sometimes do not resolve the ambiguity. With the 2000 event samples, however,the ambiguities disappear.

Recently, BABAR has made an important step to improve the constraints on α, via studying $B^0(\bar{B}^0) \to \rho^+\rho^-$ decays [14]. Using the isospin analysis they determined that the solution compatible with the SM is $\alpha = 100^\circ \pm 13^\circ$. The estimate is based on 232 million $\Upsilon(4S) \to B\bar{B}$ decays. This mode has potential show stoppers improving errors on α. The analysis assumed a 100% longitudinal polarization of the $B^0 \to \rho^+\rho^-$; if this is not true, an angular analysis is needed and requires a lot more data. However, BABAR measured the longitudinal polarization fraction $f_L = 0.978 \pm 0.014(\text{stat.})^{+0.021}_{-0.029}(\text{syst.})$ [14] which is consistent with one.

Regardless of that, the $\rho\pi$ system remains theoretically the cleanest way to extract α. Recently BABAR has performed first full time dependent Dalitz-plot analysis [14] and extracted $\alpha = (113^{+27}_{-17} \pm 6)^\circ$. In the following sections we will show how with the BTeV detector one would have significantly improved sensitivity on α using the full time-dependent Dalitz-plot analysis of the $B \to \rho\pi$ decays.

3. THE BTeV CONCEPT

BTeV was designed as a second-generation experiment to study CP violation in B decays. It would have made possible to carry out practically all measurements of CP violation and decays of the B hadrons accessible at the asymmetric B factories and at CDF and D0 running at Tevatron and it could have done those measurements at a much higher precisions. The detector design is ideally suited to study B decays containing neutral particles, especially the modes of interest here, $B^0 \to (\rho\pi)^0$.

The studies presented in [15–19] indicate that the forward direction at the Tevatron presents a number of striking advantages. First of all, there is a large

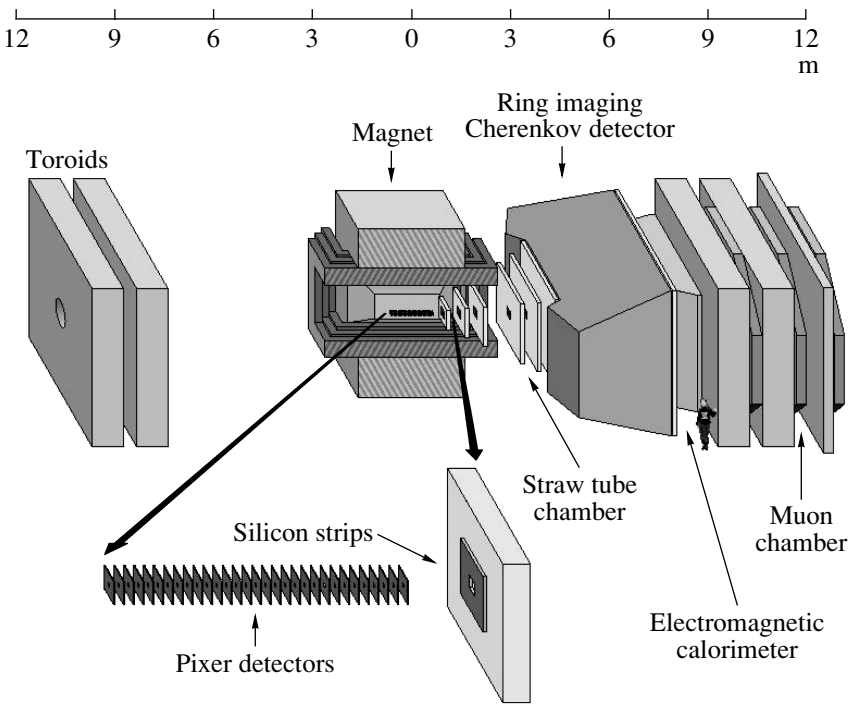

Fig. 3. Layout of the BTeV Detector.

cross section for the production of correlated $b\bar{b}$ pairs. Secondly, the B hadrons that are formed have relatively large momenta, on average 30 GeV/c, and, therefore, their decay products do not suffer much from multiple Coulomb scattering. This would allow BTeV to make precision measurements of the spatial origins of particles and as a result, BTeV would be able to determine if they arose from B hadrons that traveled on the order of several mm prior to their decays. Furthermore, the geometry was very natural for certain aspects of detector technology that significantly enhance the physics performance. For these reasons, the BTeV Collaboration designed a detector with "forward coverage."

The physics case for BTeV involves reconstructing a variety of different decay modes of the B, B_s, and other b hadrons and, in many cases, following their time evolution and tagging the flavor of the parent B at production and at the moment of decay. These decay modes may involve charged hadrons, charged leptons, photons (prompt or from π^0's), and tertiary vertices from the $b \to c$ decay chain. The product branching fractions of many decay modes of interest, including any tertiary decays, are quite small, typically 10^{-5} to 10^{-7}. This, together with the large background of minimum bias events, demanded that BTeV be able to reconstruct multibody final states, with a good resolution in invariant mass, and to handle very high data rates. In order to carry out the physics program, the detector must have the ability to separate decay vertices from the primary interaction vertex and to reconstruct secondary B vertices and daughter charm vertices. This requires a precision vertex detector. It must also be able to measure the time evolution of decays for time-dependent asymmetry studies. The most demanding requirement is to be able to follow the very rapid oscillations of the B_s meson in order to study mixing and CP violation. The detector must have the ability to distinguish pions, kaons, and protons from each other to reduce confusion among similar decays such as $B \to \pi\pi$ and $B \to K\pi$ so that decays of interest will not be contaminated by other decays, causing the resulting measurements to be diluted. Many key decay modes have π^0's, γ's, or particles that decay into them, such as ρ's or η's. Leptons, muons, and electrons (positrons) appear in many key final states, so good lepton identification is also required. Finally, many of the detector properties which are needed to isolate and reconstruct signals are also needed to perform "flavor tagging".

The BTeV detector is shown schematically in Fig. 3. The covered angular region is from approximately 10 to 300 mrad with respect to the antiproton beam. When a B decay of interest is contained within the acceptance of the detector, there is a high probability that the decay products of the coproduced $\bar{B}$ will also be within the acceptance of the detector. Furthermore, since the charged B-decay products are not degraded by multiple scattering in the detector

material, that allows accurate determination of B decay vertices.

The key design features of BTeV include:

A dipole centered at the interaction region placing a magnetic field on the vertex detector, allowing the use of momentum determination in the trigger. There are two open ends of the magnet. One open end allows particles to flow into the instrumented "arm". The field is used by the tracking system to provide precise momentum determination of all of the charged particles.

A precision vertex detector based on planar pixel arrays. The outputs are used in the trigger processor to find detached heavy-quark decay vertices in the first-level trigger. They also provide precise and unambiguous three-dimensional space points to help reconstruct charged particles.

Precision tracking using a combination of straw tubes and silicon microstrip detectors, inside the straws close to the beam line, where the charged-particle occupancies are the largest. This system, when coupled with the pixels, provides excellent momentum and mass resolution out to 300 mrad.

Excellent charged-particle identification using a Ring Imaging Cherenkov Detector (RICH). The RICH provides hadron identification from 3–70 GeV and lepton identification from 3–20 GeV, out to the full aperture of 300 mrad, which is crucial since the muon detector and calorimeter do not cover the full solid angle covered by the RICH. The RICH has two independent systems sharing the same space. One has a gas (C_4F_8O) radiator and a multianode photomultiplier photon detector, and the other has a liquid C_5F_{12} radiator and a phototube photon detector. Both systems work in the region of visible light.

A high-quality $PbWO_4$ electromagnetic calorimeter with excellent energy resolution, position resolution, and segmentation, covering up to 200 mrad, capable of reconstructing final states with single photons, π^0's, η's, or η''s, and identifying electrons.

Excellent identification of muons out to 200 mrad using a dedicated detector consisting of a steel toroid instrumented with proportional tubes. This system has the ability to both identify single muons above momenta of about 10 GeV/c and supply a dimuon trigger.

A detached vertex trigger at Level 1 using the pixel detector information, which makes BTeV efficient for most final states, including purely hadronic modes. The trigger ignores low-momentum tracks that have large multiple scattering and would thereby avoid creating false secondary vertices.

A very high-speed and high-throughput data-acquisition system which eliminates the need to tune the experiment to specific final states.

4. RECONSTRUCTION EFFICIENCIES FOR $B^0 \to (\rho\pi)^0$ DECAYS IN BTeV

As stressed earlier, measuring the time-dependent CP-violating effects in the decays $B^0 \to (\rho\pi)^0 \to \pi^+\pi^-\pi^0$ provides a theoretically clean way to determine the angle α of the UT, as shown by Snyder and Quinn [4]. We report on the expected performance of the BTeV detector for these decays, taking into account excellent reconstruction efficiency of the π^0's that is made possible with the electromagnetic calorimeter based on PWO crystals.

Excellent mass resolution in the π^0 reconstruction reduces the background significantly, particularly, near the edges of the Dalitz plot, where the $\rho\pi$ events lay. In addition, good resolution in the proper decay time is crucial to determine the angle α.

The reconstruction efficiencies for $B \to \rho\pi$ were studied using GEANT3-based simulation [20]. We generated two samples: 250 000 $\rho^\pm\pi^\mp$ and 250 000 $\rho^0\pi^0$. Both samples were generated with a mean of two Poisson-distributed non-beauty interactions per beam crossing. This number of interactions per beam crossing corresponds to running at the designed Tevatron luminosity of 2×10^{32} cm^{-2}s^{-1} and 132-ns bunch spacing. It should be mentioned that we used two separate Monte Carlo samples only to refine the selection procedure and determine the reconstruction efficiency and signal-to-background ratios. For the Dalitz-plot analysis the interference between charged and neutral ρ mesons was simulated.

The analysis relies on BTeV event reconstruction software packages, including track reconstruction based on the Kalman filter method, vertex reconstruction, and shower reconstruction.

With the use of the electromagnetic calorimeter, we would find many good π^0 candidates. Photon candidates are required to have minimum reconstructed energy of 1 GeV and pass a shower shape cut designed to reject hadronic showers. We reduce the background rate by insuring that the photon candidates are not too close to the projection of any charged tracks to the calorimeter.

Figure 4a shows a $\gamma\gamma$ invariant mass distribution of the $B \to \rho\pi$ events when the pairs have energy sum greater than 5 GeV and the vector sum of transverse momenta greater than 0.75 GeV/c^2. The π^0 signal is very clear; the π^0 mass resolution in this sample is 3.7 MeV/c^2.

Candidate π^0's are two-photon combinations with invariant masses between 125 and 145 MeV/c^2. The π^0 reconstruction efficiency depends on the distance from the beam line and is presented in Fig. 4b; the

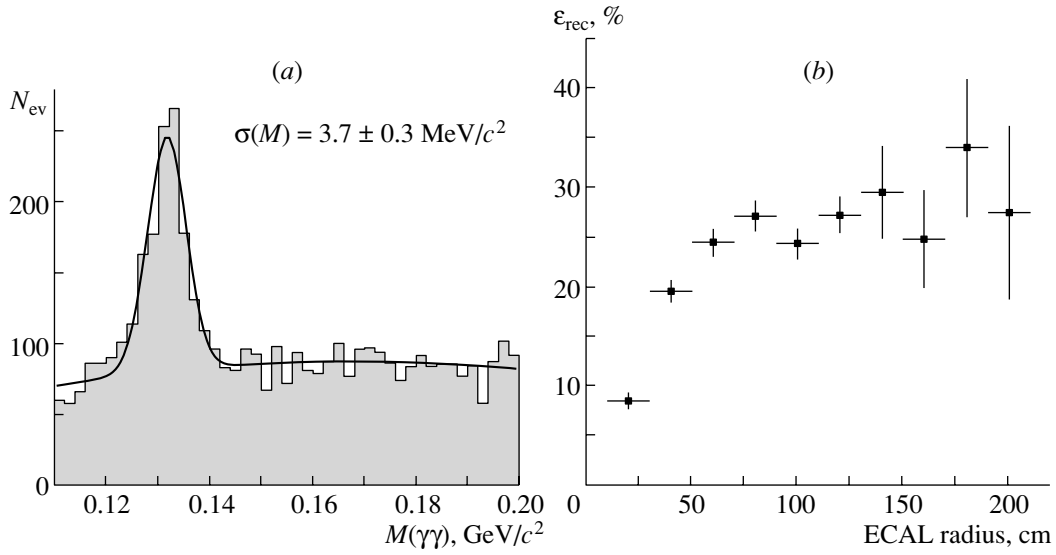

Fig. 4. (*a*) The π^0 signal in the $\gamma\gamma$ spectrum from $B^0 \to \rho^+\pi^-$ simulated events and (*b*) the efficiency of reconstructing the π^0 as a function of distance from the beam line. All events considered have at least one signal B decay. The sample includes a mean of two Poisson-distributed non-beauty interactions per beam crossing.

π^0's are taken from the $B^0 \to \rho^\pm\pi^\mp$ events; this simulation was run with a calorimeter larger than that proposed, so we could view the dependence on radius. The denominator contains all events in which the event passes the trigger, all charged tracks are reconstructed, and the combination of the two charged tracks passes some vertexing and detachment cuts. In the calculation of the efficiency we use the "right" two charged tracks. However, if a pair of good charged tracks is combined with a background π^0, it does not significantly increase the efficiency. We should mention that by further developing the π^0-reconstruction algorithm, the efficiency of π^0 reconstruction at small ECAL radia within a high particle occupancy might be increased.

We look for events containing a secondary vertex formed by two oppositely charged tracks. One of the most important selection requirements for discriminating the signal from the background is that the events have well measured primary and secondary vertices. We demand that the primary and the secondary vertices be well defined by requiring $\chi^2/\mathrm{dof} < 2$ for their vertex fits. Once the primary and the B-decay vertices are determined, the distance L between the vertices and its error σ_L are computed. The quantity L/σ_L is a measure of the significance of detachment between the primary and secondary vertices. We require $L/\sigma_L > 4$. The two vertices must also be separated from each other in the plane transverse to the beam. We define $r_{\mathrm{transverse}}$ in terms of the primary interaction vertex position (x_P, y_P, z_P) and the secondary vertex position (x_S, y_S, z_S), namely $r_{\mathrm{transverse}} = \sqrt{(x_P - x_S)^2 + (y_P - y_S)^2}$ and reject events when $r_{\mathrm{transverse}} < 0.132$ mm. Finaly, to insure that the charged tracks do not originate from the primary, we require that both the π^+ and the π^- candidates have an impact parameter with respect to the primary vertex (DCA) greater than 100 μm.

Table 1. Selection criteria (the notation is defined in the text)

Criteria	Value	Efficiency for $B \to \rho^0\pi^0$, %
Primary vertex criteria	$\chi^2 < 2$	
Secondary vertex criteria	$\chi^2 < 2$	
Normalized distance L/σ	> 4	
DCA of track [μm]	> 100	
E_{π^+} [GeV]	> 4	
E_{π^-} [GeV]	> 4	
$p_t(\pi^+)$ [GeV/c]	> 0.4	
$p_t(\pi^-)$ [GeV/c]	> 0.4	6.82
t_{proper}/t_0	< 5.5	1.51
$p_t^{\mathrm{sum}}/\Sigma p_t$	< 0.06	0.42
Distance L [cm]	< 5	0.41
E_{π^0} [GeV]	> 5	0.39
$p_t(\pi^0)$ [GeV/c]	> 0.75	0.29
Isolation for γ [cm]	> 5.4	0.24
$m_{\pi\pi}$ [GeV/c^2]	0.55–1.1	0.22
$m_{\gamma\gamma}$ [MeV/c^2]	125–145	0.19
$r_{\mathrm{transverse}}$ [cm]	0.0132	0.18

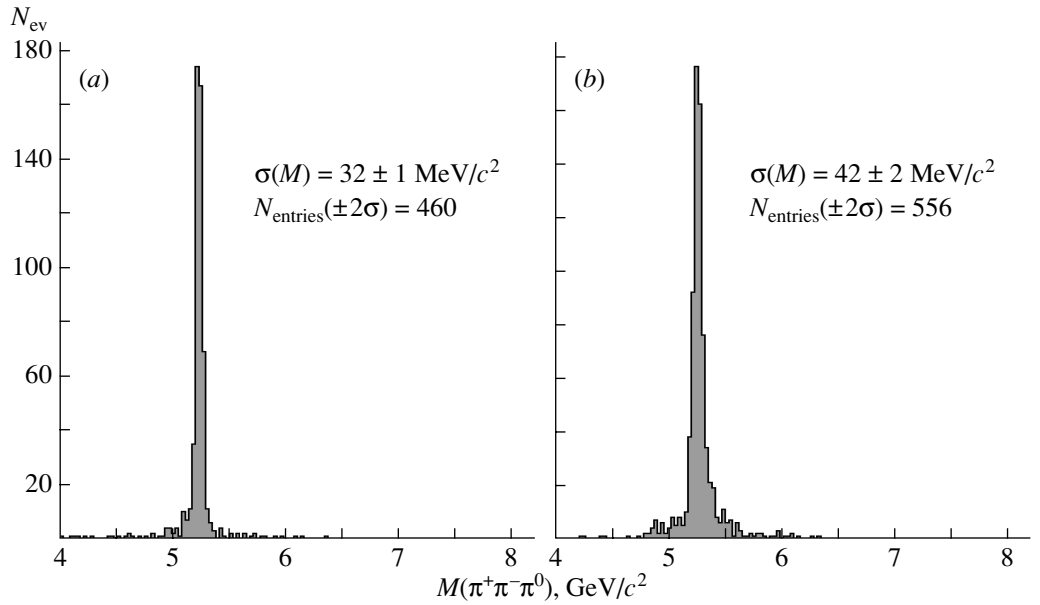

Fig. 5. Invariant mass $\pi^+\pi^-\pi^0$ (after cuts) for the simulated (*a*) $B^0 \to \rho^0\pi^0$ and (*b*) $B^0 \to \rho^+\pi^-$ decays. Each event includes on the average two Poisson distributed non-beauty interactions per beam crossing, mixed to the beauty production interaction. The number of signal event were counted as the number of entries in the $\pm 2\sigma$ interval around the B mass, minus estimated number of background entries.

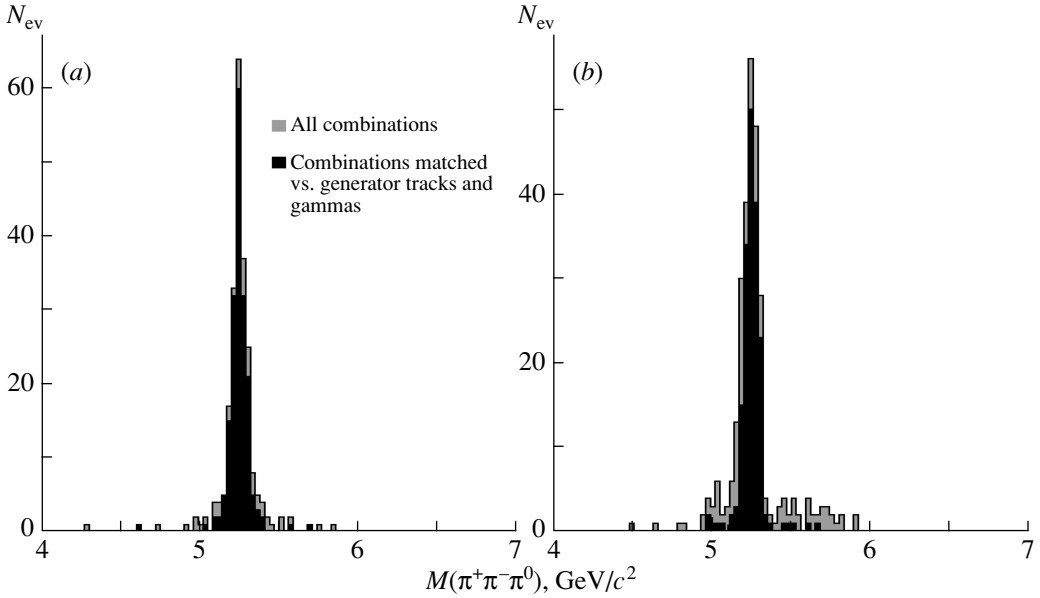

Fig. 6. Invariant mass $\pi^+\pi^-\pi^0$ (after cuts) matched vs generator tracks and photons, for the simulated $B^0 \to \rho^+\pi^-$ at (*a*) two and (*b*) six interactions per crossing.

When we calculate the invariant masses of the $\pi^+\pi^-$ and $\pi^\pm\pi^0$ pairs, we require at least one of them to be compatible with the ρ mass, that is, between 0.55 and 1.1 GeV/c^2. In addition, we use several kinematic cuts which reduce the background to $B \to \rho\pi$ without significantly decreasing the reconstruction efficiency. We require that $p_t^{\rm sum}$ divided by the scalar sum of the p_t values of all three particles, $p_t^{\rm sum}/\Sigma p_t$, be small. The vector sum $p_t^{\rm sum}$ is defined with respect to the B direction of flight which is calculated from the reconstructed primary and secondary vertices. We also make a cut on the B proper time decay requiring it to be less than 5.5 times the B^0

lifetime ($t_{\text{proper}}/t_0 < 5.5$). The selection criteria are summarized in Table 1.

After the first eight cuts the residual reconstruction efficiency was 6.82% for $B \to \rho^0\pi^0$ (see Table 1). At this stage we had $\pi^+\pi^-\pi^0$ combinations, where less than 5% of them were in the B peak and the rest was background. To kill the background, we used nine additional cuts. We can see how the reconstruction efficiency was decreasing after each cut in the right column of Table 1.

The results are shown in Fig. 5 for (*a*) $B^0 \to \rho^0\pi^0$ and (*b*) $B^0 \to \rho^+\pi^-$ Monte Carlo samples, respectively. The B^0 mass resolution in these samples is in the range 32–42 MeV/c^2. The signal interval is defined as $\pm 2\sigma$ around the B mass, minus estimated background. The reconstruction efficiency is $(0.18 \pm 0.02)\%$ for $B^0 \to \rho^0\pi^0$ and $(0.22 \pm 0.02)\%$ for $B^0 \to \rho^\pm\pi^\mp$.

Similar simulation studies were repeated with six non-beauty interations per crossing mixed to the beauty production interaction to estimate reconstruction efficiency for the $B^0 \to \rho^+\pi^-$ decay. Results were compared with those at two interactions per crossing. The statistics used to compare the two cases were 100 000 events.

At six interactions per beam crossing the B^0 mass resolution remains practicaly unchanged, as it is found to be 44 ± 3 MeV/c^2. The $B^0 \to \rho^+\pi^-$ reconstruction efficiency is estimated at $(0.2 \pm 0.02)\%$. This represents the effect of only 10% as compared to two background interactions per crossing.

However, the number of false 3π combinations that would pass the cuts appears to increase somewhat as the number of non-beauty interactions per beam crossing goes up. To prove that most of the entries in the B^0 mass region are true $\pi^+\pi^-\pi^0$ combinations coming from the B^0 decay, we have done a check against generator level information. Results of comparison are presented in Fig. 6. It is clear that the B^0 signal dominates in both distributions; false 3π combinations could, in principal, mimic the signal but most of the 3π combinations are the correct ones.

Using the previously calculated reconstruction efficiency we could expect to have ~1000 flavor-tagged $\rho^\pm\pi^\mp$ events and ~150 flavor-tagged $\rho^0\pi^0$ events per year (2×10^7 s given that BTeV was assumed to run 10 months per year). The samples would include both B^0 and $\overline{B}^0$ decays, with proper time measurements for both states.

In principal, one can use the untagged sample in the likelihood (see Section 7) to extract α. Actually, this sample does not carry any information on α but it allows to extract other parameters related to direct CP violation and helps the fit converge. This leads to an improved resolution on α when the untagged sample is utilized. However, in this paper we present results obtained only with the tagged sample.

5. SIGNAL-TO-BACKGROUND RATIO IN $B^0 \to (\rho\pi)^0$ DECAYS IN BTeV

The analysis by Snyder and Quinn [4] showed that with 2000 background-free events they could always find a solution for α. BTeV could have collected such a statistics within 4×10^7 seconds (approximately 2 yr). But we expect some background whose effects need to be estimated.

For a channel with a branching ratio of the order of 10^{-5} and efficiencies lower than 1%, it is necessary to generate at least 10^7 $b\bar{b}$ background events. For this study we generated 2×10^7 generic $b\bar{b}$ events ($B \to \rho\pi$ channels excluded) and processed them through the GEANT3-based full detector simulation. Each event contains a mean of two Poisson-distributed non-beauty interactions. Selection criteria listed in Table 1 are applied. To get the background estimate, we count all of the events between 5 and 7 GeV/c^2, then we scale that number down by the ratio of the signal region divided by the background selection region.

The results of the analysis are presented in Figs. 7*a* and 7*b*. The signal-to-background levels are approximetely 4 : 1 and 1 : 3 for $\rho^\pm\pi^\mp$ and $\rho^0\pi^0$, respectively, when there are on the average two interactions per crossing.

We have also investigated the effect of a larger number of interactions per crossing on the $\rho^+\pi^-$ background, similar to the study on the signal sample. We merged our background sample with an additional sample of non-beauty events generated with a Poisson-distributed average of four interactions per crossing. Charged tracks in the merged events were projected onto the calorimeter, and photons from both samples were added in. Thus, the full confusion of six interactions per crossing is simulated in the calorimeter. The way we did this study, the confusion is not present in the simulation of the tracking system but separate studies show that the charged particle tracking system is reasonably robust against six interactions per crossing. The analysis then proceeded as before. We have reprocessed 1.33×10^7 events and have compared the results corresponding to this statistics at two or six interactions per crossing. The background to $B^0 \to \rho^+\pi^-$ at six interactions per crossing is presented in Fig. 7*c*). We have found that at six interactions per crossing the background to $B^0 \to \rho^+\pi^-$ increased to 109 events, as compared to 56 events at two interactions per crossing. This

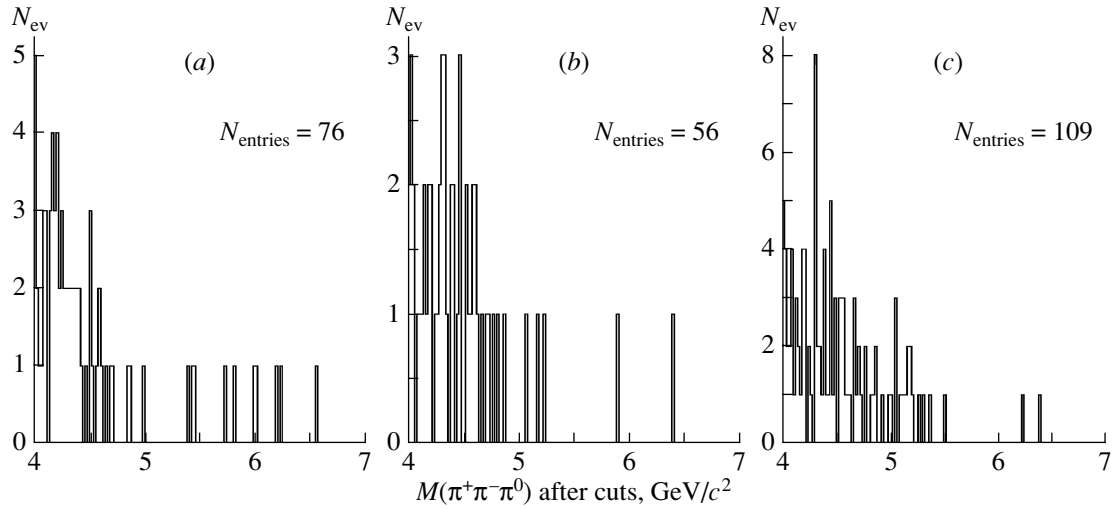

Fig. 7. Background $\pi^+\pi^-\pi^0$ invariant mass for (a) $B^0 \to \rho^0\pi^0$ and (b) $B^0 \to \rho^+\pi^-$ at two interactions per crossing, and (c) $B^0 \to \rho^+\pi^-$ at 6 interactions per crossing.

demonstrates that the background could increase at six interactions per crossing but the effect is expected to be about a factor of 2.

6. REPRESENTATION OF AMPLITUDES AND PHENOMENOLOGICAL INPUTS

6.1. Classification of the Amplitudes

In this Section we first define the formalism. Next, we estimate parameter values so that the simulation is as close as possible to reality.

Amplitudes of neutral B^0-meson decay to $\rho\pi$ are represented in the form

$$|B^0\rangle = f_i a_{ij}, \qquad \{ij\} = \{+-\}, \{-+\}, \{00\}, \quad (7)$$

$$a_{ij} = \left(-e^{-i\alpha}T_{ij} + P_{ij}\right) e^{-i\beta}, \quad (8)$$

where T_{ij} and P_{ij} give tree and penguin amplitudes, correspondingly, as depicted in Fig. 8 extracted from [21].

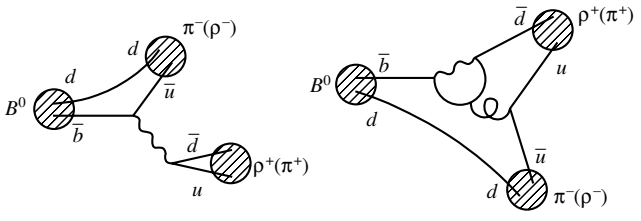

Fig. 8. (Left) The tree and (right) penguin diagrams for the $B^0 \to \rho^+\pi^-$ ($B^0 \to \rho^-\pi^+$) decays.

The f_k represents the relativistic Breit-Wigner form for $\rho \to \pi\pi$:

$$f_k = \frac{\cos(\theta_k)}{s - m_\rho^2 + i\Pi(s)}, \quad (9)$$

where s is the square of the invariant mass (π_1, π_2) and θ_k is the angle between a decay pion and the line of flight of the ρ. The function $\Pi(s)$ is defined as

$$\Pi(s) = \frac{m_\rho^2}{\sqrt{s}} \left(\frac{p(s)}{p(m_\rho^2)}\right)^3 \Gamma(m_\rho^2), \quad (10)$$

$$p(s) = \sqrt{s/4 - m_\rho^2},$$

where m_ρ is the ρ mass and Γ is the width.

The amplitudes a_{ij} for B^0 and $\overline{B}^0$ decay are written as a sum of tree (T) and penguin (P) contributions as

$$\begin{aligned} a_{+-} &= -e^{i\gamma}T^{+-} + e^{-i\beta}P^{+-}, \quad (11)\\ a_{-+} &= -e^{i\gamma}T^{-+} + e^{-i\beta}P^{-+},\\ a_{00} &= -e^{i\gamma}T^{00} + e^{-i\beta}P^{00},\\ \bar{a}_{+-} &= -e^{-i\gamma}T^{-+} + e^{i\beta}P^{-+},\\ \bar{a}_{-+} &= -e^{-i\gamma}T^{+-} + e^{i\beta}P^{+-},\\ \bar{a}_{00} &= -e^{-i\gamma}T^{00} + e^{i\beta}P^{00}, \end{aligned}$$

where γ and β are the usual CKM angles and $\alpha + \beta + \gamma = \pi$. Using both isospin symmetry and the fact that the penguin amplitude is a pure $\Delta I = 1/2$ transition leads to the replacement

$$P_{00} = -\frac{1}{2}\left(P_{+-} + P_{-+}\right). \quad (12)$$

For the tree diagrams after Fierz transformation one naively gets

$$T_{00} = \frac{1}{2}\frac{a_2}{a_1}\left(T_{+-} + T_{-+}\right), \qquad (13)$$

where factors $a_{1,2}$ represent contributions due to gluon corrections to the weak interactions of quarks and depend on renormalization scale. The corresponding Lagrangian is approximated by

$$\mathcal{L} = \frac{G_{\rm F}}{2\sqrt{2}} V_{ud}V_{ub}^* C_\pm (\bar{b}_i \mathcal{O}_\mu u^j)(\bar{u}_k \mathcal{O}^\mu d^l) \qquad (14)$$
$$\times \left[\delta_j^i \delta_l^k \pm \delta_l^i \delta_j^k\right],$$

where indices mark $SU(3)$ colors, and the factors are defined as

$$a_1 = \frac{1}{2N_c}[C_+(N_c+1) + C_-(N_c-1)], \qquad (15)$$
$$a_2 = \frac{1}{2N_c}[C_+(N_c+1) - C_-(N_c-1)],$$

where $N_c = 3$. In the limit of neglecting the gluon corrections we get

$$C_\pm = 1, \qquad a_1 = 1, \qquad a_2 = 1/N_c.$$

However, the corrections taking into account the renormalization-group dependence on a decay scale put the ratio a_2/a_1 to a negative value approximately given by

$$\frac{a_2}{a_1} = -0.25 \pm 0.05. \qquad (16)$$

In fact, as was shown in [22] and [23], expressions (15) following from the factorization hypothesis can be significantly modified by "non-factorizable effects" in the complex phase. This means that only the absolute value of the ratio

$$\left|\frac{a_2}{a_1}\right| = 0.25 \pm 0.05$$

is reliable. The value of the phase is not realiably predicted by the theory but is roughly estimated to be about 45°.

Corrections in (12) and (13) due to isospin symmetry breaking are considered to be negligible [21] and they are not included in the following simulations.

6.2. Phenomenological Constraints on the Parameters

A phenomenological analysis of possible values for the amplitudes in (7) has been performed in [21] and [24]. It is based on a global fit to the measured rates assuming $SU(3)$-flavor symmetry for $B \to \rho\pi$, $B \to K^*\pi$, and $B \to \rho K$ decays. The analysis gives approximately twice enhancement of penguin amplitudes in comparison with QCD expectations [23]. The preferable values of amplitudes with theoretical expectations of uncertainties are summarized in Table 2, which has two sets of parameters we use in our modelling of the signal.

Table 2. Amplitudes in units of T_{+-} set to 1 and expected uncertainties from fits in [21] and [24]

Parameter	Set I	Set II	Theoretical uncertainty or limits
$\lvert T_{-+}\rvert$	0.8	0.8	0.63–0.9
$\arg[T_{-+}]$	$-20°$	$-20°$	$\pm 10°$
$\lvert P_{+-}\rvert$	0.18	0.18	± 0.05
$\arg[P_{+-}]$	30°	30°	$\pm 30°$
$\left\lvert\frac{P_{-+}}{T_{-+}}\right\rvert$	0.28	0.28	0.14–0.32
$\arg[P_{-+}/T_{-+}]$	80°	130°	$\pm 60°$
$\lvert a_2/a_1\rvert$	0.25	0.25	0.18–0.32
$\arg[a_2/a_1]$	45°	45°	$0-2\pi$
α	88°	100°	80°–110°

The value of $|T_{-+}|$ is ordinary fixed by the factorization hypothesis [21], so that it is equal to the ratio of decay constants $f_\pi/f_\rho \approx 0.63$, while the ratio fitted by $SU(3)$ ansatz results in a greater value of about 0.7. Nevertheless, we fix this parameter to 0.8, reproducing the mean magnitude of branching fractions. The uncertainties of complex phases are not given explicitly in [21] and [24], but we expect them to be lower than 30° at fixed absolute values of penguin-to-tree ratios. The amplitude of $B^0 \to \rho^0\pi^0$ is constructed in accordance with (12), (13), and (16).

Now we make the transition to the estimate of parameter values in the simulation and to the comparison with the existing experimental results.

The overall normalization is tuned to the experimental sum of CP-averaged branching ratios

$$\mathcal{B}_{\rho\pi}^{\pm\mp} = \mathcal{B}_{\rho\pi}^{+-} + \mathcal{B}_{\rho\pi}^{-+} = (24.0 \pm 2.5) \times 10^{-6},$$

where

$$\mathcal{B}_{\rho\pi}^{+-} = \frac{1}{2}\left\{\mathcal{B}[B^0 \to \rho^+\pi^-] + \mathcal{B}[\bar{B}^0 \to \rho^-\pi^+]\right\}$$
$$= (13.9 \pm 2.2) \times 10^{-6},$$
$$\mathcal{B}_{\rho\pi}^{-+} = \frac{1}{2}\left\{\mathcal{B}[B^0 \to \rho^-\pi^+] + \mathcal{B}[\bar{B}^0 \to \rho^+\pi^-]\right\}$$
$$= (10.1 \pm 2.1) \times 10^{-6}.$$

For example, taking the set I of parameters we get

$$\mathcal{B}[B^0 \to \rho^+\pi^-] = 16.5 \times 10^{-6},$$

$$\mathcal{B}[B^0 \to \rho^-\pi^+] = 14.1 \times 10^{-6},$$
$$\mathcal{B}[B^0 \to \rho^0\pi^0] = 0.9 \times 10^{-6},$$

and

$$\mathcal{B}[\bar{B}^0 \to \rho^+\pi^-] = 4.6 \times 10^{-6},$$
$$\mathcal{B}[\bar{B}^0 \to \rho^-\pi^+] = 11.6 \times 10^{-6},$$
$$\mathcal{B}[\bar{B}^0 \to \rho^0\pi^0] = 1.4 \times 10^{-6},$$

which should be compared with experimental averages from BELLE, BABAR, and CLEO in [21] and [24]

$$\mathcal{B}[B^0 \to \rho^+\pi^-] = (16.5^{+3.1}_{-2.8}) \times 10^{-6},$$
$$\mathcal{B}[B^0 \to \rho^-\pi^+] = (15.4^{+3.2}_{-2.9}) \times 10^{-6},$$

and

$$\mathcal{B}[\bar{B}^0 \to \rho^+\pi^-] = (4.8^{+2.6}_{-2.3}) \times 10^{-6},$$
$$\mathcal{B}[\bar{B}^0 \to \rho^-\pi^+] = (11.4^{+2.8}_{-2.6}) \times 10^{-6}.$$

The above branching ratios give CP-averaged values of

$$\mathcal{B}^{+-}_{\rho\pi} = 14.0 \times 10^{-6}, \quad \mathcal{B}^{-+}_{\rho\pi} = 9.3 \times 10^{-6}$$

for the charged modes, while for the neutral mode we have

$$\mathcal{B}^{00}_{\rho\pi} = \frac{1}{2}\left\{\mathcal{B}[B^0 \to \rho^0\pi^0] + \mathcal{B}[\bar{B}^0 \to \rho^0\pi^0]\right\} = 1.2 \times 10^{-6},$$

are consistent with the experimental value

$$\mathcal{B}^{00}_{\rho\pi} = (1.7 \pm 0.8) \times 10^{-6} < 2.5 \times 10^{-6} \text{ at } 95\% \text{ C.L.}$$

Note, that the neutral CP-averaged mode weakly depends on the complex phase of a_2/a_1, but branching ratios of B^0 and $\bar{B}^0$ strongly depend on that phase: for instance, putting $\arg[a_2/a_1] = \pi$ gives $\mathcal{B}[B^0 \to \rho^0\pi^0] = 2.1 \times 10^{-6}$ and $\mathcal{B}[\bar{B}^0 \to \rho^0\pi^0] = 0.2 \times 10^{-6}$.

The time-dependent CP asymmetry is given by

$$a^{\pm}_{CP} = \frac{\Gamma(\overline{B}^0(t) \to \rho^\pm\pi^\mp) - \Gamma(B^0(t) \to \rho^\pm\pi^\mp)}{\Gamma(\overline{B}^0(t) \to \rho^\pm\pi^\mp) + \Gamma(B^0(t) \to \rho^\pm\pi^\mp)} \quad (17)$$
$$= (S_{\rho\pi} \pm \Delta S_{\rho\pi})\sin(\Delta m_d t) - (C_{\rho\pi} \pm \Delta C_{\rho\pi})\cos(\Delta m_d t).$$

In this formula $S_{\rho\pi}$ and $C_{\rho\pi}$ represent mixing-induced CP violation and flavor-dependent direct CP violation, respectively. The value of $\Delta S_{\rho\pi}$ and $\Delta C_{\rho\pi}$ are CP conserving. The $\Delta C_{\rho\pi}$ characterizes the asymmetry between rates $\Gamma(B^0 \to \rho^+\pi^-) + \Gamma(\overline{B}^0 \to \rho^-\pi^+)$ and $\Gamma(B^0 \to \rho^-\pi^+) + \Gamma(\overline{B}^0 \to \rho^+\pi^-)$ at $t = 0$, i.e., at initial moment of evolution, while $\Delta S_{\rho\pi}$ indicates mixing of decays at $t \neq 0$, and as we have found, it strongly depends on both the relative strong phase of penguin with respect to tree amplitude in $\rho^-\pi^+$ mode (the parameter $\arg[P_{-+}/T_{-+}]$) and the CKM angle α.

Time-integrated asymmetries are given by

$$A^{+-}_{\rho\pi} = -\frac{A_{\rho\pi} + C_{\rho\pi} + A_{\rho\pi}\Delta C_{\rho\pi}}{1 + \Delta C_{\rho\pi} + A_{\rho\pi}C_{\rho\pi}} = \frac{N(\overline{B}^0 \to \rho^-\pi^+) - N(B^0 \to \rho^+\pi^-)}{N(\overline{B}^0 \to \rho^-\pi^+) + N(B^0 \to \rho^+\pi^-)}, \quad (18)$$

$$A^{-+}_{\rho\pi} = -\frac{A_{\rho\pi} - C_{\rho\pi} - A_{\rho\pi}\Delta C_{\rho\pi}}{1 - \Delta C_{\rho\pi} - A_{\rho\pi}C_{\rho\pi}} = \frac{N(\overline{B}^0 \to \rho^+\pi^-) - N(B^0 \to \rho^-\pi^+)}{N(\overline{B}^0 \to \rho^+\pi^-) + N(B^0 \to \rho^-\pi^+)}, \quad (19)$$

$$A_{\rho\pi} = \frac{|a_{+-}|^2 + |\bar{a}_{+-}|^2 - |a_{-+}|^2 - |\bar{a}_{-+}|^2}{|a_{+-}|^2 + |\bar{a}_{+-}|^2 + |a_{-+}|^2 + |\bar{a}_{-+}|^2}, \quad (20)$$

where non-zero values of $A^{+-}_{\rho\pi}$ and $A^{-+}_{\rho\pi}$ indicate direct CP violation.

In Table 3 we show a comparison between observable quantities obtained by using I- and II-set values with experimental data.

The comparison shows that the range of parameters we use seem to be reasonable.

7. TIME-DEPENDENT DALITZ PLOT ANALYSIS OF $B^0 \to (\rho\pi)^0$ DECAYS IN BTeV

In Section 4 we demonstrated that BTeV would be able to collect a sample of ~1000 flavor-tagged $B^0 \to (\rho\pi)^0$ events within one year of operation, which would allow a reliable Dalitz-plot analysis of this decay mode.

The model of the Dalitz-plot analysis has three parts: $B \to \rho\pi$ signal, random true ρ plus random true π, the "resonant background", uniform density, the "non-resonant background".

The formalism used to fit the Dalitz plot is based on 13 independent parameters: 6 amplitudes, 6 strong phases, and the weak phase α itself. Using the constrainst given in Eqs. (11) and (12) we can reduce the number of parameters to 11. We fix a reference rate and strong phase so that the total number of parameters reduces to 9. Two additional parameters must be added if we allow the resonant and non-resonant background fractions to be determined by the fit.

Due to the low reconstruction efficiency of this particular final state it would not be feasible to include the Snyder-Quinn formalism directly into the full detector Monte Carlo simulation: it would have required

Table 3. A comparison of values of quantities evaluated from sets I and II with available experimental data from [24]

Quantity, units	Set I	Set II	Experimental data
$\mathcal{B}[B^0 \to \rho^+\pi^-] \times 10^{-6}$	16.5	16.5	$16.5^{+3.1}_{-2.8}$
$\mathcal{B}[B^0 \to \rho^-\pi^+] \times 10^{-6}$	14.1	14.3	$15.0^{+3.2}_{-2.9}$
$\mathcal{B}[B^0 \to \rho^0\pi^0] \times 10^{-6}$	0.9	0.6	$1.7 \pm 0.8(\mathcal{B}^{00}_{\rho\pi})$
$\mathcal{B}[\bar{B}^0 \to \rho^+\pi^-] \times 10^{-6}$	4.6	6.6	$4.8^{+2.6}_{-2.3}$
$\mathcal{B}[\bar{B}^0 \to \rho^-\pi^+] \times 10^{-6}$	11.6	11.4	$11.6^{+2.8}_{-2.6}$
$\mathcal{B}[\bar{B}^0 \to \rho^0\pi^0] \times 10^{-6}$	1.4	1.8	$1.7 \pm 0.8(\mathcal{B}^{00}_{\rho\pi})$
$A_{\rho\pi}$	-0.100	-0.054	-0.114 ± 0.067
$S_{\rho\pi}$	-0.15	-0.30	-0.13 ± 0.18
$\Delta S_{\rho\pi}$	0.33	0.35	0.33 ± 0.18
$C_{\rho\pi}$	0.33	0.27	0.35 ± 0.14
$\Delta C_{\rho\pi}$	0.24	0.16	0.20 ± 0.14
$A^{+-}_{\rho\pi}$	-0.17	-0.18	-0.18 ± 0.14
$A^{-+}_{\rho\pi}$	-0.51	-0.37	$-0.52^{+0.18}_{-0.20}$
α	88°	100°	$100^{\circ\,+12^\circ}_{-10^\circ}$, (CKM unitarity: $98^\circ \pm 16^\circ$)

significant computer power and the generation of a huge number of events to obtain the desired statistics.

We have opted for a different approach. The generated template events are distributed flat over the Dalitz-plot domain, with the exponential time distribution and random tag $= \pm 1$. We further use a rejection algorithm based on the isospin amplitudes formalism for the tree and the penguin contributions to the Dalitz plot.

Time evolution of the $B^0 \to (\rho\pi)^0$ decay amplitudes, including $B-\bar{B}$ mixing, is given by:

$$\mathcal{A} = e^{-\Gamma t/2}\left(\cos\frac{\Delta M t}{2}|B^0\rangle + i\frac{q}{p}\sin\frac{\Delta M t}{2}|\overline{B}^0\rangle\right), \tag{21}$$

$$\overline{\mathcal{A}} = e^{-\Gamma t/2}\left(i\frac{p}{q}\sin\frac{\Delta M t}{2}|B^0\rangle + \cos\frac{\Delta M t}{2}|\overline{B}^0\rangle\right), \tag{22}$$

where $|B^0\rangle$ is given by Eq. (7). The template events are accepted or rejected based on whether a random number is less than or greater than $|\mathcal{A}|^2/|\mathcal{A}_{\max}|^2$.

The background has been parametrized to account for both non-resonant and resonant components. The non-resonant background has been uniformly distributed over the Dalitz-plot domain. The resonant background allows the two pions to have a Breit–Wigner-shaped enhancement with the ρ-line shape.

The process of reconstruction of the accepted events is simulated by smearing them using the resolutions on momentum reconstruction and lifetime. These values were obtained from the simulation described in Section 4. The smearing has been computed comparing the reconstructed momentum, of π^+, π^-, and π^0 to the generator information, $\sigma(p_{\rm gen} - p_{\rm rec})/p_{\rm gen} = 0.7\%$ for charged pions and at 0.9% for π^0's. Signal events are generated with an exponential time distribution. The rejection algorithm appropriately shapes the time evolution of the B^0's according to mixing and CP violation. The resolution on lifetime has also been estimated to be 64 fs using the Monte Carlo described in Section 4, by computing the reconstructed lifetime and comparing it to the generated one. It should be pointed out that the resolution on lifetime is independent of lifetime. Proper time-dependent acceptance was included in the likelihood. The background level is determined by a full GEANT simulation of 20 000 000 generic $b\bar{b}$ events; it is assumed that this background has an exponential time dependence given by the average lifetime of b-flavored hadrons.

We have used two values for α: $\alpha = 88^\circ$ and $\alpha = 100^\circ$. For each case we have generated 500 independent trials, starting with different random numbers every time. Every trial contains 1000 signal events, 250 non-resonant background events, and 250 resonant background events. This corresponds to one year (2×10^7 s) of data taking. The background level

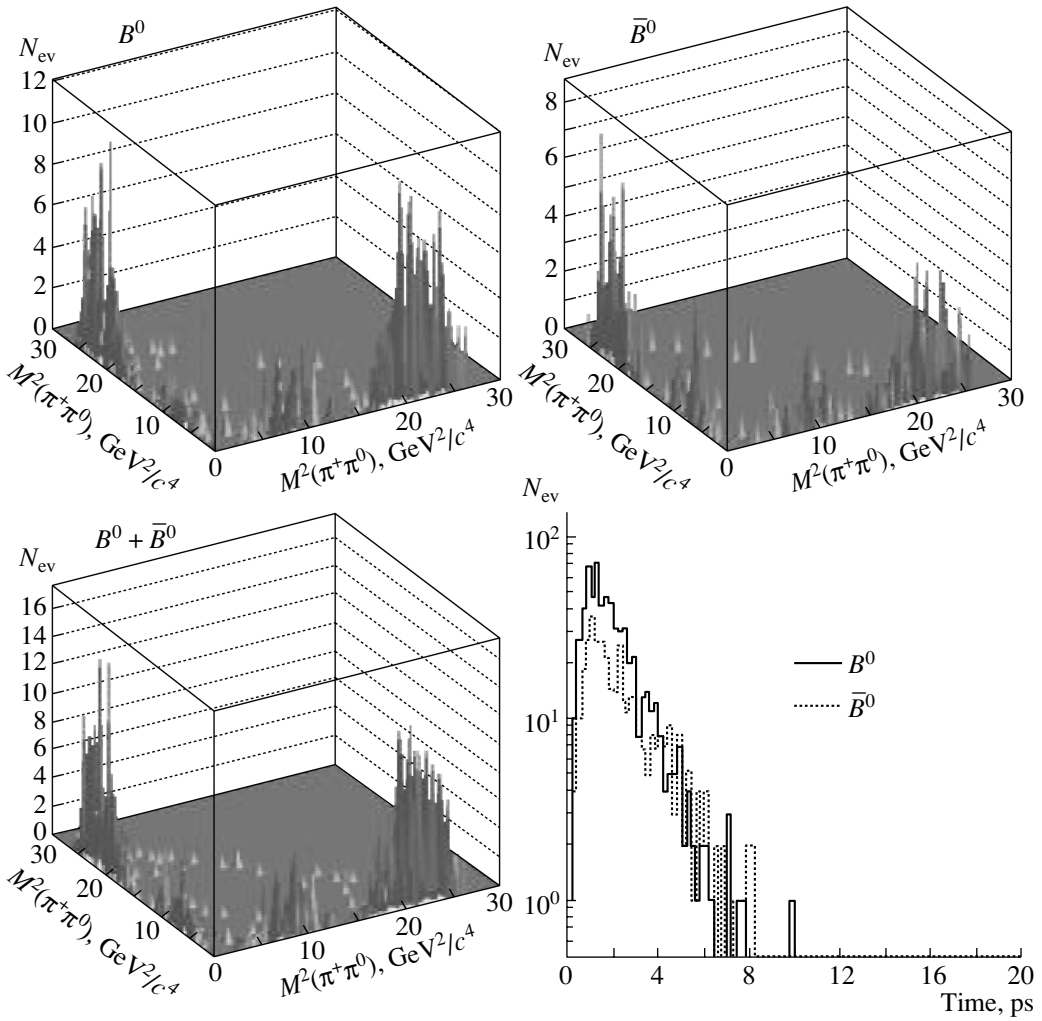

Fig. 9. Dalitz plot and proper time distribution for one trial of 1000 events for $\alpha = 88^\circ$ (detector efficiency included).

was chosen based on the Monte Carlo studies described in Section 5, for the case of of running at 396-ns bunch spacing (six interactions per beam crossing), which would be BTeV's most challenging scenario. The Dalitz plot for one such sample is shown in Fig. 9.

To extract the parameters and the associated errors we have used an unbinned maximum likelihood fit. The likelihood over the full Dalitz domain is given by

$$-2\ln\mathcal{L} = -2\sum_{i=1}^{N_{B_d^0}} \ln\frac{\mathcal{F}_i}{1+R_{\rm non}+R_{\rm res}} - 2\sum_{j=1}^{N_{\overline{B}_d^0}} \ln\frac{\overline{\mathcal{F}_j}}{1+R_{\rm non}+R_{\rm res}}, \quad (23)$$

where

$$\mathcal{F}_i = \frac{|\mathcal{A}(s_i^+, s_i^-, t_i, \alpha, \ldots)|^2}{\mathcal{N}(\alpha,\ldots)}\varepsilon(s_i^+, s_i^-) + \left[R_{\rm non}\frac{1}{\mathcal{N}_t} + R_{\rm res}\frac{|{\rm BW}(s_i^+, s_i^-)|^2}{\mathcal{N}_{\rm BW}}\right]\varepsilon(s_i^+, s_i^-), \quad (24)$$

$$\overline{\mathcal{F}}_j = \frac{|\overline{\mathcal{A}}(s_j^+, s_j^-, t_j, \alpha, \ldots)|^2}{\mathcal{N}(\alpha,\ldots)}\varepsilon(s_j^+, s_j^-) + \left[R_{\rm non}\times\frac{1}{\mathcal{N}_t} + R_{\rm res}\frac{|{\rm BW}(s_j^+, s_j^-)|^2}{\mathcal{N}_{\rm BW}}\right]\varepsilon(s_j^+, s_j^-). \quad (25)$$

Here, $s_j^+ = (m_{\pi^+} + m_{\pi^0})_j^2$ and $s_j^- = (m_{\pi^-} + m_{\pi^0})_j^2$ are two Dalitz plot variables for the jth event; $N_{B_d^0}$ and $N_{\overline{B}_d^0}$ are the total number of the B_d^0 and $\overline{B}_d^0$ events, BW is a generic from for a relativistic Breight–Wigner. The normalization $\mathcal{N} = (|\mathcal{A}|^2 + |\overline{\mathcal{A}}|^2)\varepsilon$ is integrated over the Dalitz plane and over the

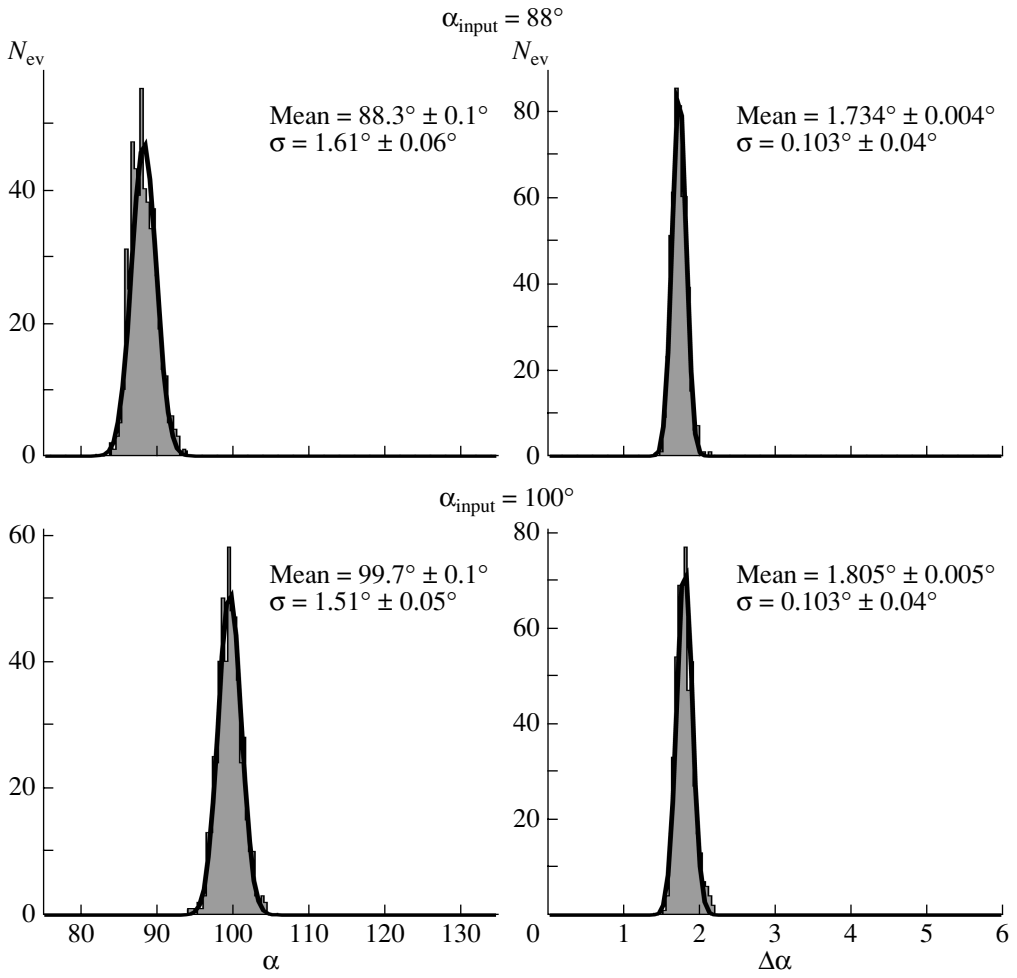

Fig. 10. Accuracy in determining α: fit value of α and deviation $\Delta\alpha$ from input value ($\alpha_{\text{input}} - \alpha_{\text{fit}}$).

proper time and weighted by the detector efficiency. R_{non} and R_{res} are defined as

$$R_{\text{non}} = \frac{N_{\text{non}}^{\text{back}}}{N_{B_d^0+\overline{B}_d^0}^{\text{signal}}} \quad R_{\text{res}} = \frac{N_{\text{res}}^{\text{back}}}{N_{B_d^0+\overline{B}_d^0}^{\text{signal}}}. \qquad (26)$$

The fit has been performed for 500 samples, for each input value of $\alpha = 88°$ and $\alpha = 100°$, to confirm the stability of the procedure. The results of the fit value for α and its deviation $\Delta\alpha$ from the input value are presented in Fig. 10, for the input values of $\alpha = 88°$ (sample 1) and $\alpha = 100°$ (sample 2). We measured $\alpha = 88.3 \pm 1.6°$ and $\Delta\alpha = 1.7 \pm 0.09°$ for sample 1 and $\alpha = 99.7 \pm 1.5°$ and $\Delta\alpha = 1.8 \pm 0.1°$ for sample 2, which is in good agreement with the input parameters.

These results have been obtained for ideal tagging. We have also made fits for different errors in the tagging dilution factor. The results are presented in Table 4 in the range from almost ideal $\sigma_{\text{dil}} = 2\%$ to the very conservative $\sigma_{\text{dil}} = 25\%$. The displacements can be considered as systematic errors and should be summed with the ideal tagging error in quadrature. Assuming that the error in the tagging dilution factor in BTeV would have been 10–15%, we estimate the accuracy in measuring α at 1.8–2.3° for $\alpha = 88°$ and 3.4–4.7° for $\alpha = 100°$. We consider the most conservative case, a 15% error on the dilution factor for $\alpha = 100°$, and conclude that BTeV could measure α with the accuracy of better that 5° in one year of operation.

In order to ensure that our event generation model is correct (see Eqs. (17)–(20)) we have integrated Eq. (23) over the Dalitz-plot domain, so that only the proper time dependence of the B-meson decay rate is left. We fit the data with the assumption of the time-dependent CP asymmetry of the B-meson decay as expressed in Eq. (16). The CP asymmetries a_{CP}^{+} for $\rho^+\pi^-$ and a_{CP}^{-} for $\rho^-\pi^+$ (see Eq. (17)) are shown in Fig. 11: the solid curves represent the fit results. The results obtained for the parameters in Eq. (17) are:

$$S_{\rho\pi} = -0.22 \pm 0.06(-0.15), \qquad (27)$$

Table 4. The change of the value of the α coming out of the likelihood fit at different errors in the tagging dilution factor

Input α, deg	Additional displacement, deg					
	σ_{dil}, %					
	2	5	10	15	20	25
88	+1.0	+0.4	−0.6	−1.6	−2.7	−3.9
100	−0.9	−1.6	−2.9	−4.3	−5.8	−7.2

$$\Delta S_{\rho\pi} = 0.29 \pm 0.06(0.33), \quad (28)$$

$$C_{\rho\pi} = 0.38 \pm 0.05(0.34), \quad (29)$$

$$\Delta C_{\rho\pi} = 0.24 \pm 0.05(0.23), \quad (30)$$

where the numbers in parentheses represent the input to the simulation.

The results of the fit are in good agreement with the input values used in the Monte Carlo simulation. This justifies the validity of the model we used to extract α and demonstrates that these important parameters could have been measured with the accuracy of 0.05–0.06 in one year of BTeV operation. As one can see in Table 3, up until now these values are known only crudely.

8. COMPARISON ON α SENSITIVITY WITH LHCb

Towards the end of the decade, LHCb will go into operation with similar capabilities for all-charged states, but will not have a high-quality electromagnetic calorimeter. The LHCb Collaboration has estimated [25] that in one year of data taking they could achieve an accuracy σ_α/α better than 10%, which is twice worse than in BTeV, where σ_α/α was expected to be better than 5%. Let us consider the origin of such a difference.

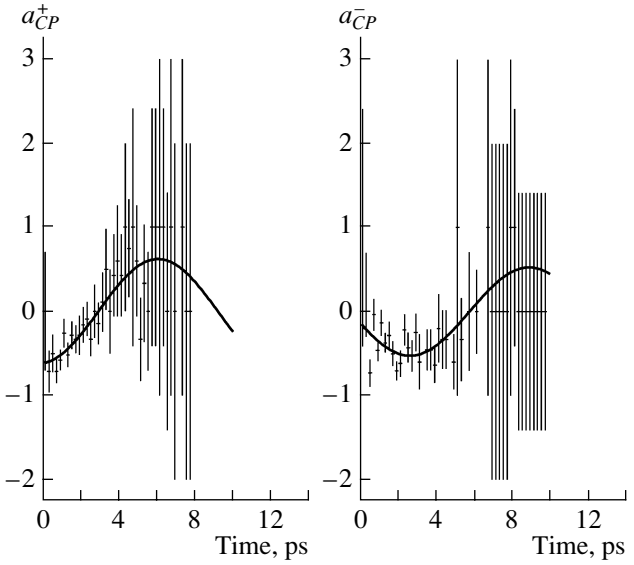

Fig. 11. CP asymmetries a^+_{CP} for $\rho^+\pi^-$ and a^-_{CP} for $\rho^-\pi^+$. The solid curves represent the fit.

LHCb started with the benchmark configuration, which they defined as a pure $B_d \to 3\pi$ sample free from any experimental effects except for the proper time acceptance. They came up with ≈1.2% accuracy in α. After they had included the effect of tagging efficiency and the associated wrong-tag fraction, the α resolution degraded to ≈4.0%. When including the Dalitz-plot acceptance, the α resolution degraded to ≈5.7%. When they did not use the un-tagged sample, the resolution degraded to 7.2%. At the end, they considered the various effects of a background contamination with the nominal background-to-signal ratio $B/S = 0.8$, and the α resolution has finally degraded to ≈10%.

BTeV has made a likelihood fit with the all expected experimental resolutions including background contamination with the BTeV nominal $B/S = 0.25$, but for ideal tagging. The result was $\sigma_\alpha/\alpha \approx 1.8\%$. Considering the most conservative case, a 15% error on the dilution factor, they concluded that BTeV could measure α with an accuracy of better than 5%.

So we can see that one of the main origins of a difference in the α sensitivities in BTeV and LHCb is a significant advantage in a quality of the BTeV electromagnetic calorimeter. BTeV would have had a better background rejection due to excellent π^0-mass resolution. BTeV also expected a higher yield and a lower B/S due to the calorimeter performance. In one year of data taking BTeV would have expected 1200 flavor-tagged signal events with $B/S = 0.25$, while LHCb only 600 flavor-tagged signal events with $B/S \approx 1$. However, there are some more origins of the difference. The LHCb low-level trigger, the higher LHCb energy, and the high track density in LHCb should also play a role. Finally, different scenario the both experiments used for their input parameters (tree and penguin amplitudes and phases) could also explain a part of the difference.

9. CONCLUSIONS

Physics simulations of the decay $B \to \rho\pi$ for the BTeV project at Fermilab has been performed. The main idea was to estimate the expected accuracy in extracting the angle α of the UT.

To calculate the signal-to-background ratio for the decay of interest, 2×10^7 background events were simulated and processed through the full detector

simulation based on GEANT3 package. Using the excellent electromagnetic calorimeter based on lead tungstate crystals, the $B^0 \to \rho^+\pi^-$ decay the signal-to-background ratio is estimated at 4 : 1 or 2 : 1, for 132-ns or 396-ns beam crossing intervals, respectively.

A phenomenological analysis has been made for the possible values of tree and penguin amplitudes and phases for the process of interest, based on a global fit with $SU(3)$-flavor asymmetry for $B \to \rho\pi$, $B \to K^*\pi$ and $B \to \rho K$. The latest experimental data from BABAR and BELLE were used in this analysis.

Dalitz-plot analysis of the $B \to \rho\pi$ decay with input from the phenomenological analysis has been presented. It has been shown that in one year of data taking BTeV could achieve the accuracy better than 5° on the angle α.

The interference between tree and penguin diagrams can be exploited by measuring the time-dependent CP-violating effects in the $B \to \rho\pi$ decays. In this paper it has been found that mixing-induced CP-violation parameter $S_{\rho\pi}$ and flavor-dependent direct CP-violating parameter $C_{\rho\pi}$ could be measured with the accuracy of 0.05–0.06.

This work was partially supported by the U.S. National Science Foundation and the Department of Energy, the Russian Ministry of Education and Science, and INTAS Ref. No. 05-103-7571. We thank Alexander Bondar, Olivier Deschamps, and Daniele Pedrini for fruitfull discussions.

REFERENCES

1. P. Langacker, in *CP Violation* (World Sci., Singapore, 1989), p. 552.
2. N. Cabibbo, Phys. Rev. Lett. **10**, 531 (1963); M. Kobayashi and K. Maskawa, Prog. Theor. Phys. **49**, 652 (1973).
3. A. Kulyavtsev et al., *Proposal for an Experiment to Measure Mixing, CP Violation and Rare Decays in Charm and Beauty Particle Decays at the Fermilab Collider—BTeV, 2000*; G. Y. Drobychev et al., *Update to Proposal for an Experiment to Measure Mixing, CP Violation and Rare Decays in Charm and Beauty Particle Decays at the Fermilab Collider—BTeV, 2002*.
4. A. E. Snyder and H. R. Quinn, Phys. Rev. D **48**, 2139 (1993).
5. A. Bevan, hep-ex/0411090.
6. L. Wolfenstein, Phys. Rev. Lett. **51**, 1945 (1983).
7. S. Stone, in *St. Croix 1996, Techniques and Concepts of High-Energy Physics IX*, NATO ASI Series (Plenum, New York, 1996), p. 465; hep-ph/9610305.
8. B. Aubert et al. (BABAR Collab.), hep-ex/0408127.
9. K. Abe et al. (BELLE Collab.), Phys. Rev. D **71**, 072003 (2005); hep-ex/0408111.
10. The Heavy Flavor Averaging Group, http://www.slac.stanford.edu/xorg/hfag/ (Summer 2003 and Winter 2004 averages).
11. M. Gronau, Phys. Rev. Lett. **63**, 1451 (1989); M. Gronau and D. London, Phys. Rev. Lett. **65**, 3381 (1990).
12. The theoretical accuracy of this approach is limited by electroweak penguins, that are expected to be rather small in this case. In principle, they can be taken into account, as pointed out by A. J. Buras and R. Fleischer, Eur. Phys. J. C **11**, 93 (1999); hep-ph/9810260; M. Gronau, D. Pirjol, and T.-M. Yan, Phys. Rev. D **60**, 034021 (1999); hep-ph/9810482.
13. H. J. Lipkin, Y. Nir, H. R. Quinn, and A. Snyder, Phys. Rev. D **44**, 1454 (1991).
14. B. Aubert et al. (BABAR Collab.), hep-ex/0408099; B. Aubert et al. (BABAR Collab.), hep-ex/0503049.
15. F. Abe et al., CDF/PUB/BOTTOM/PUBLIC/3759, submitted to ICHEP'96, and references therein; F. Abe et al., Phys. Rev. Lett. **75**, 1451 (1995).
16. R. Abbott et al., Phys. Lett. B **487**, 264 (2000); hep-ex/9905024; S. Abachi et al., Phys. Rev. Lett. **74**, 3548 (1995).
17. M. Mangano, P. Nason, and G. Ridolfi, Nucl. Phys. B **373**, 295 (1992).
18. I. Redondo, in *Proceedings of the workshop for Monte Carlo Generators for HERA Physics, 1998/99,* http://www.desy.de/ heramc/proceedings/wg60; E. Norrbin and T. Sjostrand, in *Proceedings of the workshop for Monte Carlo Generators for HERA Physics, 1998/99*, http://www.desy.de/ heramc/proceedings/wg60.
19. M. Artuso, in *B Decays,* 2nd ed. (World Sci., Singapore, 1994).
20. *GEANT: CERN Program Library Writeup W5013,* http://wwwinfo.cern.ch/asdoc/geant_html3/geantall.html.
21. M. Gronau and J. Zupan, hep-ph/0407002.
22. M. Beneke, G. Buchalla, M. Neubert, and C. T. Sachrajda, Nucl. Phys. B **606**, 245 (2001); hep-ph/0104110; M. Neubert, hep-ph/0012204.
23. M. Beneke and M. Neubert, Nucl. Phys. B **675**, 333 (2003); hep-ph/0308039.
24. J. Charles et al. (CKMfitter Group), hep-ph/0406184.
25. O. Deschamps, P. Perret, and A. Robert, LHCb 2005-024, PHYS (2005).